Stability of the Class II Classified Product Crystallizer with Fines Removal

The stability of crystal-size distribution (CSD) in the classified product crystallizer with fines removal was investigated using spectral techniques to determine stable solutions of the linearized population balance. The model used to describe the crystallizer assumed rapid growth kinetics (high yield), magma-dependent secondary nucleation, and recycle of dissolved fines. Fines removal and classified product removal were characterized in the model by piece-wise constant removal rates ($R - 1$) and z times the MSMPR removal rate, respectively.

Stability regions were presented as critical values of the kinetic nucleation/growth rate exponent $i = d(\log B^0)/d(\log G)$ versus dimensionless parameters of the system. The parameters which influence CSD stability were maximum fines size and removal rate, product classification size and removal rate, and the magma-characterizing exponent in the nucleation expression. Whether or not dissolved fines are recycled directly back to the crystal magma also influences stability.

ALAN D. RANDOLPH
GARY L. BEER

Chemical Engineering Department

and

JAMES P. KEENER

Mathematics Department
University of Arizona
Tucson, Arizona 85721

SCOPE

Fines destruction, classified product removal, and clear liquor advance (growth type operation) are three process configurations that can be achieved in a commercial crystallization machine with current technology. Product classification can be externally imposed (for example, wet screens, cyclones, elutriators) or inadvertently occurs in a mixed magma vessel because of nonisokinetic product removal. Ironically, product size increases brought about by fines destruction may increase product classification of the larger-sized particles at the point of removal, thus reducing the size improvement expected from theoretical considerations. The net result is that a narrower more attractive CSD is produced, but the problem of cycling is aggravated. Figure 1 illustrates the idealization to be used in this study of such a complex crystallization process.

Randolph and Larson (1971, p. 142) discuss the so-called "$R - z$ crystallizer model" (see Figure 1) in which fines are assumed to be removed, dissolved, and recycled in the size range 0, L_F at a rate $R - 1$ times the MSMPR rate while product in the size range L_p, ∞ is removed at a rate z times the MSMPR value. Product in the size range 0, L_p is assumed to be removed at the MSMPR rate. Clarified liquor can be advanced to increase solids concentration. This idealized, yet realistic, model of a complex crystallizer captures the essence of what can be done with current technology.

The purpose of this study is to evaluate the stability of Class II classified crystallizers with a fines dissolver and present the results in terms of the $R - z$ crystallizer model. Realistic magma-dependent nucleation kinetics are assumed and the solute recycle from the fines dissolver is taken into account.

CONCLUSIONS AND SIGNIFICANCE

A linearized stability analysis of the classified product crystallizer with fines removal was performed using spectral analysis techniques to characterize stability regions of the linearized partial differential equation describing the system. Results were presented in terms of the four dimensionless parameters, R, z, x_F, and x_p of the so-called "$R - z$ crystallizer model."

Fines removal as small crystals (a negligible fraction of dissolved fines compared to production rate) lowers the nucleation/growth rate sensitivity ratio at the point of instability. However, sensitivity ratios of about 15 to 20 would still be required to produce instability for reasonable levels of fines removal. Fines removal as larger crystals (an appreciable fraction of production dissolved in the fines destruction system) stabilizes CSD. Fines removal by itself cannot account for the low-order CSD cycling sometimes observed in commercial machines unless the increased supersaturation levels caused by fines removal creates discontinuous jumps in nucleation rate (for example, sudden appearance of homogeneous nucleation).

Classified product removal (that is, accelerated removal of particles greater than some product size L_p) significantly destabilizes CSD. Increases in classification ratio beyond 5 to 6 do not contribute further to CSD instability while classification at lower product sizes greatly destabilizes CSD. Product classification could account for the low-order cycling sometimes observed in commercial machines. The combination of product classification with fines removal at small particle size in the $R - z$ crystallizer configuration increases the likelihood of CSD cycling; combined fines destruction and nonisokinetic product removal could well account for low-order cycling. Further, production of larger sized crystals by excessive fines destruction increases the likelihood of classification at the point of removal.

Stabilization of CSD in a cycling crystallizer of the

type studied might be achieved by lowering the fines removal rate while increasing the fines size (hence increasing the mass of crystals dissolved at constant λ) or by closer approaching the ideal of iso-kinetic mixed product withdrawal. Alternately, stabilization might be achieved by dissolving fines at a dimensionless size in excess of say $x_F = 0.3$ with recycle of the dissolved solute to a feed make-up tank rather than back to the crystal magma (assuming that total feed concentration would be maintained constant). The large fines flow rate might make this technique impractical, however, unless the fines were first concentrated.

Crystal-size distribution (CSD) is an important property of an operating crystallizer; dynamics of CSD cause operating difficulties as well as off-specification product. Thus, transient and unstable CSD's represent a significant industrial problem which has received considerable attention. The long retention times typical of crystallizers aggravate this problem.

It would be wise to distinguish between CSD transients and instability. Dynamics of the former type are caused by outside crystallizer upsets (for example dilution addition, feed rate or composition change, partial fouling of the apparatus, etc.) while an unstable CSD results from the particular form of crystallizer configuration and the operating parameters imposed on the given system kinetics.

In terms of the dynamic CSD equations one can say that transients result from time-dependent outside forcing functions while instability results from the structure of the equations. Sustained limit-cycle solutions to these equations is a possibility due to a unique process feedback occurring in self-seeded crystallizers. This process feedback is discussed extensively by Randolph and Larson (1971) and results from the fact that crystallization is an area-dependent mass transfer process. As the crystal area available for transport changes due to CSD dynamics, the necessary supersaturation levels change, thus affecting nucleation levels and hence CSD.

Many industrial crystallizers have fast growth kinetics and hence maintain high yield (that is, $[C_i - C]/[C_i - C_s] \approx 1$) even when CSD cycles. Such crystallizers, identified as Class II systems, can be described by a constraint on the crystal growth rate (Randolph and Larson, 1971, p. 83) rather than writing detailed solute balances in terms of a concentration variable. This constraint can be written as

$$G(t) = \frac{P_I(t)}{\left(\frac{\rho V}{2}\right) A(t)} \tag{1}$$

That is, the level of growth rate in a Class II system is forced rapidly by the system kinetics to a level proportional to the internal rate of make and inversely to the crystal surface area. The variable $P_I(t)$ is generally considered as an outside disturbance while $A(t)$ is determined by the current CSD. Nuttall in Randolph and Larson (1971, p. 97) shows that $P_I(t)$ also changes with changing CSD in a crystallizer with a fines dissolver if the dissolved fines are recycled directly to the system to make over-all feed concentration time-dependent, that is, $C_i(t)$. The Class II mass balance constraint showing explicitly the rate of make perturbations due to recycle of dissolved fines for the idealized crystallizer shown in Figure 1 is

$$G = \frac{P_E + Q\rho k_v (R-1) \int_0^{L_F} nL^3\, dL}{\frac{\rho V A}{2}} \tag{2}$$

This situation is typical in industrial practice and greatly aggravates the period of transient CSD after outside process upsets. In a Class II system this recycled solute is immediately converted to an equivalent mass of solids spread over the existing surface area. Perturbations in the growth rate to accomplish this change of internal make rate occur simultaneously with changes in fines mass going to the dissolver. In a Class I system perturbations of dissolved fines mass partition between crystal solids and solute concentration according to the growth kinetics of the system. Previous linearized stability studies have neglected feed rate disturbances caused by recycle of dissolved fines; CSD instability is predicted solely on the area/supersaturation/growth rate/nucleation rate feedback interrelationship.

PREVIOUS WORK

Much elegant work on the problem of CSD instability has been published. This work is summarized in Randolph and Larson (1971, Ch. 5). Most studies have considered limiting cases of one type or another and the result is that troubleshooting, if not quantitative engineering analysis, of cycling crystallizers of industrial importance can now be achieved.

Randolph (1962) studied dynamics of CSD in a Class II MSMPR crystallizer and derived the now classic stability constraint that

$$\frac{d(\log B^0)}{d(\log G)} < 21 \tag{3}$$

for a stable CSD. Note that this result is independent of the specific form of nucleation/growth rate kinetics. Recent work in secondary nucleation kinetics indicate simple power-law expressions of the form

$$B^0 = k_N(T, RPM) M_T^j G^i \tag{4}$$

are satisfactory to correlate nucleation data from MSMPR crystallizers. Solids concentration remains constant in the dynamic Class II MSPR crystallizer. Thus, for such systems, with nucleation kinetics given by Equation (4), the stabil-

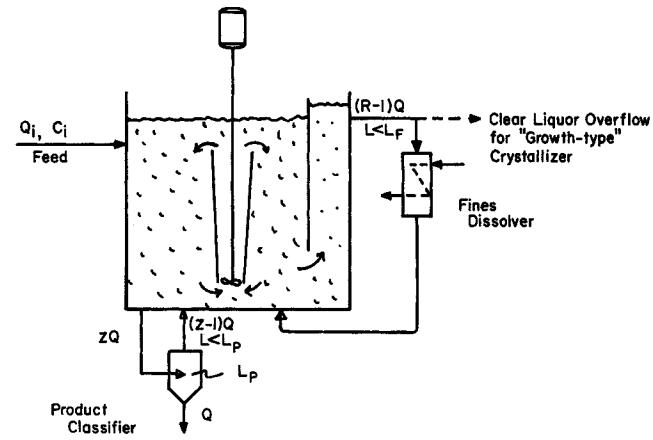

Fig. 1. Idealized model of R-z fines dissolver/classified product crystallizer.

TABLE 1. SUMMARY OF PREVIOUS WORK ON THE PROBLEM OF CSD STABILITY

	Class I system	Fines mass recycle	Void fraction-dependent nucleation	Magma-dependent nucleation	Classified product removal	Fines removal
Randolph (1962)	No	No	No	No	No	No
Randolph and Larson (1971)	No	No	No	Yes	No	Yes
Hulburt and Stefango (1969)	Yes	No	Yes	No	No	Yes
Sherwin, Shinnar and Katz (1969)	Yes	No	Yes	No	Yes	No
Lei, Shinnar and Katz (1968)	Yes	No	Yes	No	No	Yes
Present work	No	Yes	No	Yes	Yes	Yes

ity criterion becomes $i < 21$. Randolph and Larson (1971, p. 231) consider stability of a Class II MSMPR crystallizer with magma-dependent nucleation kinetics correlated with the first and fourth moments of the CSD, respectively. Only a slight relaxation of the $i < 21$ stability criterion was predicted. As the exponent i is frequently in the range of 1 to 3, it is difficult to conceive of an unstable MSMPR crystallizer unless supersaturation levels (perhaps by an extremely large or small retention time) are forced to a region where a discontinuity in nucleation rate occurs and inequality (3) is violated.

Solids concentration does cycle in a classified product removal crystallizer. Sherwin, Shinnar, and Katz (1969) describe the dynamics of an ideally classified crystallizer with no product draw-off up to size L_p and instantaneous removal thereafter. Nucleation rate was assumed to be independent of solids concentration [tantamount to $j = 0$ in Equation (4)]. Only the aforementioned supersaturation feedback relationship was used to predict instability of CSD. However, total nucleation in this model depended on void fraction and hence stability was a function of void fraction as well as relative nucleation/growth rate kinetics. Threshold stability levels of $i = 2$ were predicted with reasonable slurry densities. This study well illustrated that the form of the CSD equations was more important than kinetics in producing a cycling CSD; extreme classification could account for such behavior with realistic nucleation/growth rate kinetics.

Hulburt and Stefango (1969) studied CSD dynamics in a double-drawoff crystallizer. Such crystallizers having a more or less clear overflow (largest particles up to some size L_F) and mixed suspension underflow are industrially used to augment both particle size and solids concentration. A nucleation/growth rate model yielding both Class I and Class II (in the limit of rapid growth) systems was considered. The double-drawoff crystallizer can be thought of as a low-performance fines trap where fines are advanced from the system rather than destroyed. Relative sensitivity of nucleation/growth rate at the point of CSD instability was found to depend weakly on the clear overflow rate and size of particles removed; nucleation/growth rate sensitivity [the parameter i in Equation (4)] of about 20 was necessary to cause an unstable CSD. The critical nucleation/growth rate sensitivity passed through a minimum as yield increased from zero to 100% (extreme Class I behavior to Class II limit). However, even the lowest calculated sensitivity values did not explain low-order CSD cycling.

Lei, Shinnar, and Katz (1971) presented a stability analysis of a mixed crystallizer with a fines trap. Stability increased as maximum fines removal size increased at a constant fraction of surviving nuclei. For a point fines trap, that is, particles removed at a size negligibly small compared to product size, the modified Class II MSMPR stability criterion

$$\frac{d(\log B^0)}{d(\log G)} < 21 - \lambda \qquad (5)$$

was presented where $e^{-\lambda}$ was the fraction of original nuclei surviving the fines trap. Again, these calculations do not predict nor explain low sensitivity CSD instability.

Lei et al. (1971) in a second paper apply the same stability analysis to regulation of a fines-trap crystallizer. Direct feedback control of such systems is not feasible until a rapid in situ technique for measurement of small particle populations is developed.

Table 1 displays the key modeling assumptions that have been used previously in the study of CSD stability. These model assumptions are compared with those of the present study.

All of the references cited attack the problem with a somewhat similar approach. A lumped solute mass balance is combined with the distributed population balance for the crystals. The solute balance becomes a constraint on growth rate if a Class II system is assumed. Moments of the population balance are then taken converting the partial differential equation to a set of ordinary differential equations. These equations (with the mass balance and kinetics equations) are then linearized and regions of stability determined using classical linear analysis. Alternatively, the original distributed population balance may be linearized and stability examined by spectral techniques.

DEVELOPMENT OF EQUATIONS

The Class II $R - z$ steady state CSD equation for the crystallizer configuration shown in Figure 1 can be solved analytically (this is about as far as one can go in generality and still retain analytical CSD expressions) and are summarized in dimensionless form as follows. Power-law nucleation kinetics of the form $B^0 = k_N M_T^j G^i$ are used in this formulation.

$$\begin{aligned} \overline{y_1} &= \exp[-Rx] && x \text{ in } (0, x_F) \\ \overline{y_2} &= \exp[-(R-1)x_F]\exp(-x) && x \text{ in } (x_F, x_p) \\ \overline{y_3} &= \exp[(z-1)x_p - (R-1)x_F]\exp(-zx) && x > x_p \end{aligned} \qquad (6)$$

where $x_F = \dfrac{L_F}{G\tau}$ $x_p = \dfrac{L_p}{G\tau}$

Figure 2 plots this dimensionless population density. The Class II growth rate constraint is given in terms of the external production rate as

$$G = \left(\frac{P_E}{6QD_p}\right)^{\frac{1-j}{i+3}} (6D)^{\frac{-j}{i+3}} (k_N \rho k_v \tau^4)^{-\frac{1}{i+3}}$$

where

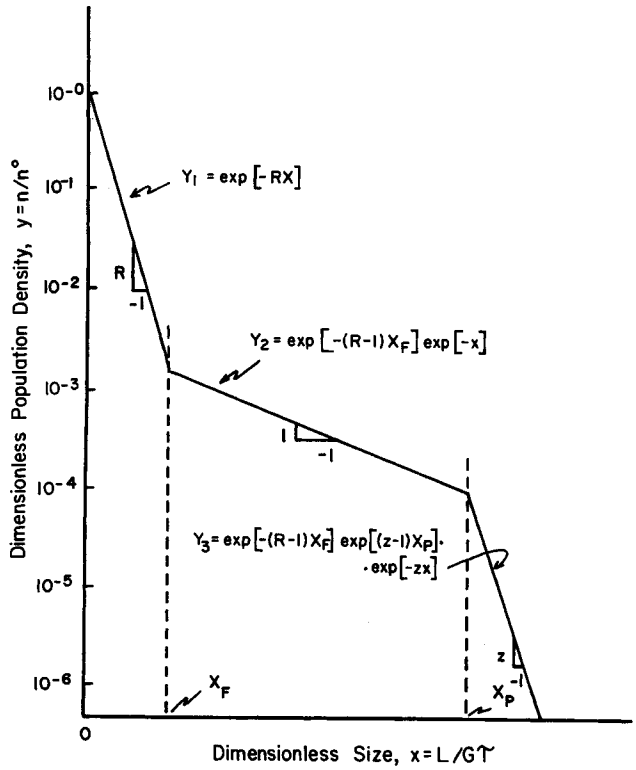

Fig. 2. Steady state population distribution for the idealized crystallizer.

$$D_p(G) = \frac{w(Rx_F)}{R^4} + \exp\left[-(R-1)x_F\right]\left[w(x_p) - w(x_F)\right] + \frac{1}{z^3}\cdot\exp\left[(z-1)x_p - (R-1)x_F\right]\left[1 - w(zx_p)\right] \quad (7)$$

with the dimensionless arguments x_F and x_p as above and where $w(p)$ is the dimensionless gamma distribution $1/6\int_0^p x^3 e^{-x}\,dx$. The dimensionless function $D(G)$ is identical to $D_p(G)$ except $1/z^4$ replaces $1/z^3$ in the last term. The value of G as given by (7) above must be solved by trial-and-error techniques by knowing the independent system inputs R, z, L_F, and L_p. This value of the growth rate is equal to that given by Equation (2); the steady state external production constraint forces growth rate to high enough values to compensate for additional internal rate of make as fines are dissolved and recycled.

These equations follow the general algorithm of simultaneous solution of mass and population balances together with system kinetics and an idealized description of the process configuration. Note that the particular power-law kinetics used for nucleation rate depend explicitly on the solids concentration but not void fraction.

The complete set of dynamic CSD equations can be set down as follows:

Population balance

$$\frac{\partial n}{\partial t} + G\frac{\partial n}{\partial L} + \frac{Q(L)n}{V} = 0 \quad (8)$$

Mass balance constraint

$$G = \frac{P_e + (R-1)Q\rho k_v \int_0^{L_F} nL^3\,dL}{\left(\frac{\rho V}{2}\right)A}$$

End condition

$$n^0 = n(0,t) = B^0/G \quad (9)$$

Nucleation kinetics

$$B^0 = k_N M_T^j\, G^i \quad (10)$$

These equations are made nondimensional and normalized by dividing by their steady state values. These dimensionless transformations are given as

$$y = n/n_0^0,\ y^0 = n^0/n_0^0\,\phi = G/G_0,\ x = \frac{LQ}{VG_0} \quad (11)$$

$$\theta = \frac{tQ}{V},\ f_{j,k} = \frac{\int_0^{L_k} L^j n\,dL}{\int_0^{L_k} L^j n_0\,dL},\ h = \frac{Q(L)}{Q},\ \bar{y} = y(x,0),$$

In terms of dimensionless variables the set of dynamic CSD equations becomes

$$\left\{\begin{array}{l} \dfrac{\partial y}{\partial\theta} + \phi\dfrac{\partial y}{\partial x} + hy = 0 \\ \\ \phi = \dfrac{1+\beta f_{3,1}}{1+\beta}\cdot\dfrac{1}{f_2} \\ \\ y^0 = f_3^j\,\phi^{i-1} \end{array}\right\} \quad (12)$$

The steady state solution $\bar{y}$ is given by Equations (6) and (7). In the above, β is the ratio of fines mass dissolved to external production, given as

$$\beta = \frac{(R-1)}{6D_p}\int_0^{x_F} x^3\,\bar{y}\,dx \quad (13)$$

Equations (12) are nonlinear and are linearized by standard perturbation techniques, taking advantage of the unity value of all normalized steady state variables to give the following linearized set in terms of small perturbations from steady state. Thus

$$\left.\begin{array}{l} \dfrac{\partial y}{\partial\theta} - \left(\dfrac{\beta}{1+\beta}\right)h\bar{y}\,f_{3,1} + h\bar{y}\,f_2 + \dfrac{\partial y}{\partial x} + hy = 0 \\ \text{with B.C.} \\ y^0 = j\,f_3 + \left(\dfrac{i-1}{1+\beta}\right)\beta\,f_{3,1} - (i-1)\,f_2 \end{array}\right\} \quad (14)$$

Equation set (14) represents the linearized dynamics of the Class II crystallizer of arbitrary process configuration [given by the removal probability function $h(x)$] with magma-dependent nucleation kinetics and accounting for a fraction $\beta/1+\beta$ of total internal production rate recycled from a fines dissolver.

The stability of this linearized set was determined in terms of relative nucleation/growth rate sensitivity i for reasonable ranges of the system parameters R, z, x_F, x_p for the $R-z$ fines removal/classified product crystallizer. The stability analysis follows closely the spectral technique of Lei et al. and is detailed in the Appendix. The characteristic equation of Equation (14) is given in terms of the $R-z$ crystallizer and kinetic parameters as

$$Y_\infty^3\,Y_{x_F}^3\left[(i-1)\,H_\infty^2 + G_\infty^2 + Y_\infty^2\right] - \left(\frac{\beta}{1+\beta}\right)Y_\infty^2\,Y_\infty^3\left[(i-1)\,H_{x_F}^3 + G_{x_F}^3\right]$$

(Equation continued on next page)

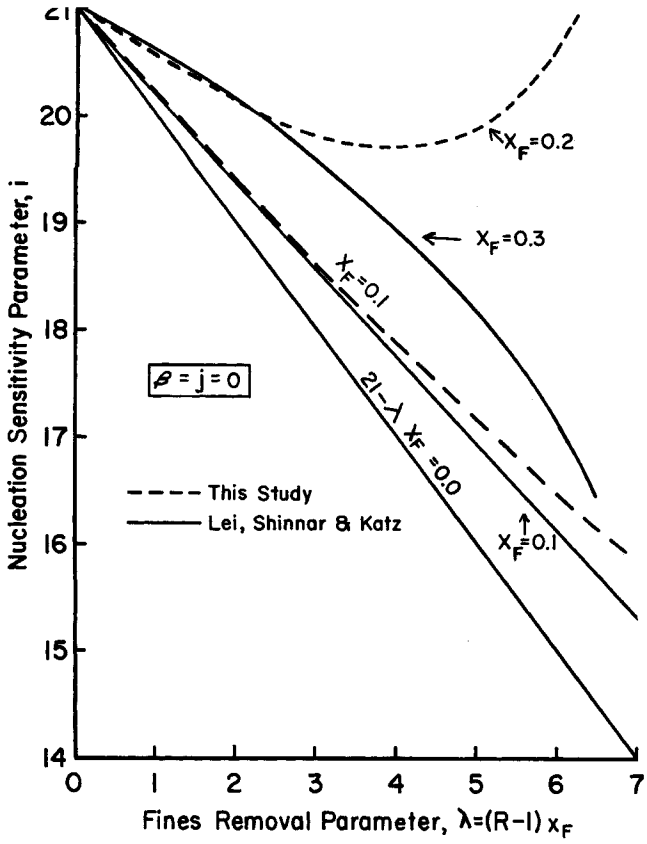

Fig. 3. Effect of fines removal on CSD stability.

$$-j\,Y_\infty^2\,Y_{x_F}^3\,H_\infty^3 - j\,Y_{x_F}^3 \begin{vmatrix} G_\infty^2 & H_\infty^2 \\ G_\infty^3 & H_\infty^3 \end{vmatrix}$$

$$+ j\left(\frac{\beta}{1+\beta}\right) Y_\infty^2 \begin{vmatrix} H_\infty^3 & G_\infty^3 \\ H_{x_F}^3 & G_{x_F}^3 \end{vmatrix} = 0 \quad (15)$$

where the variables shown are complicated integrals of the removal function $h(x)$ and steady state distribution $\overline{y}(x)$. These functions are defined as follows:

$$H_\alpha^n = \int_0^\alpha x^n H(x)\,dx \quad H(x) = \exp\left[sx - \int_0^x h(\tau)\,d\tau\right]$$

$$G_\alpha^n = \int_0^\alpha x^n G(x) H(x)\,dx$$

$$G(x) = \int_0^x h(\tau)\,e^{-s\tau}\,d\tau \quad (16)$$

$$Y_\alpha^n = \int_0^\alpha x^n \overline{y}\,dx \qquad \overline{y} = \text{steady-state } R-z \text{ distribution}$$

Equation (15), in the case of $\beta = j = 0$ (that is, magma-independent nucleation kinetics with mass recycle from the dissolver not accounted for) yields a simpler characteristic equation as follows:

$$(i-1)\,H_\infty^2 + G_\infty^2 + Y_\infty^2 = 0 \quad (17)$$

Equation (17) can be compared to the characteristic equation (in the limit for Class II behavior) studied by Lei et al., thus

$$(i-1)\,H_\infty^3 + G_\infty^3 = 0 \quad (18)$$

The difference in characteristic equations in this work and Lei et al. results because Lei et al. included void fraction (and hence the third moment) in their nucleation model.

The stability of Equation set (14) was studied by examining the characteristic equation for purely imaginary roots, $s = \sqrt{-1}\,b$. Fortunately, the kinetic sensitivity parameter i could be factored out yielding a complex equation of the form

$$i - 1 = Re\,[H_\alpha^n(b),\ G_\alpha^n(b),\ Y_\alpha^n(b)] + \sqrt{-1}\,Im\,[H_\alpha^n(b),\ G_\alpha^n(b),\ Y_\alpha^n(b)] \quad (19)$$

As the kinetic sensitivity must surely be a real number, a trial-and-error search on b was made until

$$I_m(b) = 0 \quad (20)$$

yielding

$$i = 1 + Re(b)$$

All calculations were done using complex arithmetic in FORTRAN IV on a digital computer.

STABILITY RESULTS

The characteristic equation representing the case for magma-independent nucleation and neglecting solute recycle from the fines dissolver, given by Equation (17), was first evaluated for unstable roots to determine stability regions for various parameter values of the $R-z$ crystallizer. This crystallizer model is identical to that of Lei et al. in the limit of Class II behavior except for nucleation rate assumed independent of void fraction ϵ. Recent work in measurement of secondary nucleation kinetics indicates that nucleation rate would depend on magma concentration rather than void fraction. The removal function $h(x)$ was extended to include classified product removal. Thus the removal function $h(x)$ is given for the $R-z$ crystallizer as

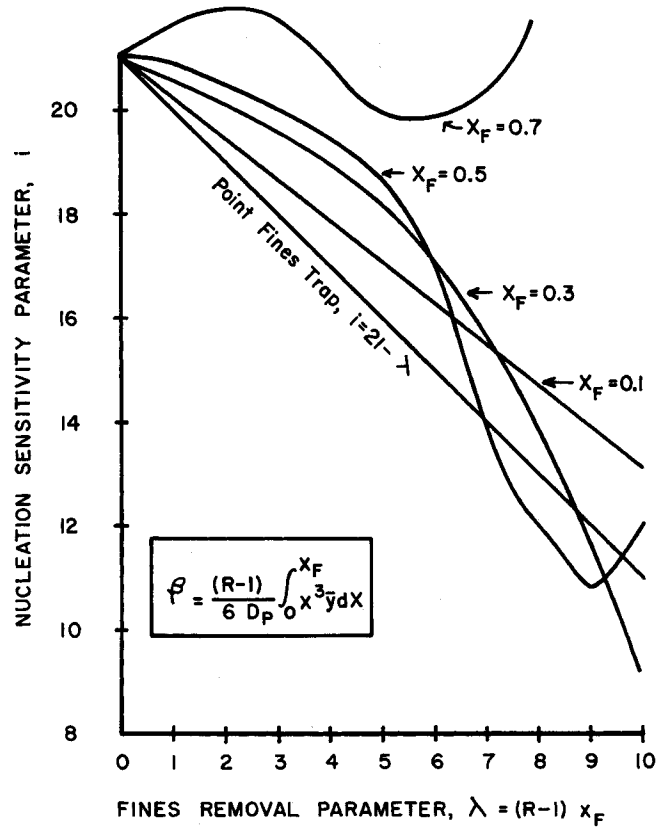

Fig. 4. Effect of fines removal on CSD stability: recycle of dissolved fines.

$$h(x) = \begin{cases} R & x \text{ in } (0, x_F) \\ 1 & x \text{ in } (x_F, x_p) \\ z & x \text{ in } (x_p, \infty) \end{cases} \qquad (21)$$

The effects of magma-influenced nucleation and solute recycle from the fines dissolver were then studied by assuming various values for the magma exponent j and calculating β from the problem parameters.

Effect of Fines Removal

Figure 3 illustrates the effects of fines removal on CSD stability predicted for the case of $j = \beta = 0$ for various levels of the dissolving parameter λ and maximum fines size x_F. The results of Lei et al. for Class II behavior are shown for comparison. Both models predict the theoretical stability limit $i = 21 - \lambda$ for the point fines trap, that is, fines dissolved at negligible size (and hence negligible mass). As the mass of dissolved crystals increases, CSD is stabilized relative to the point fines case. Figure 3 indicates that as x_F increases to above say 0.3, total stabilization of the CSD occurs. This result only holds true for the case of no recycle of the dissolved fines solute.

Figure 4 shows similar results for the case of dissolved fines recycled to the crystallizer. The extreme stabilization of CSD is not observed in this case except at large fines size and high removal rates. These results are quite similar to those predicted from the model of Lei et al.

Figure 5 better illustrates the stabilization of CSD occurring with large fines size, high removal rates, and recycle of dissolved fines. Fines removal at dimensionless sizes greater than about $x_F = 0.8$ totally stabilize CSD. The results shown in Figures 4 and 5 were unaffected by secondary nucleation kinetics represented by nonzero values of j in the nucleation model. This result is to be expected as any mass dissolved in the fines removal system is recycled and immediately precipitated due to the rapid Class II growth kinetics.

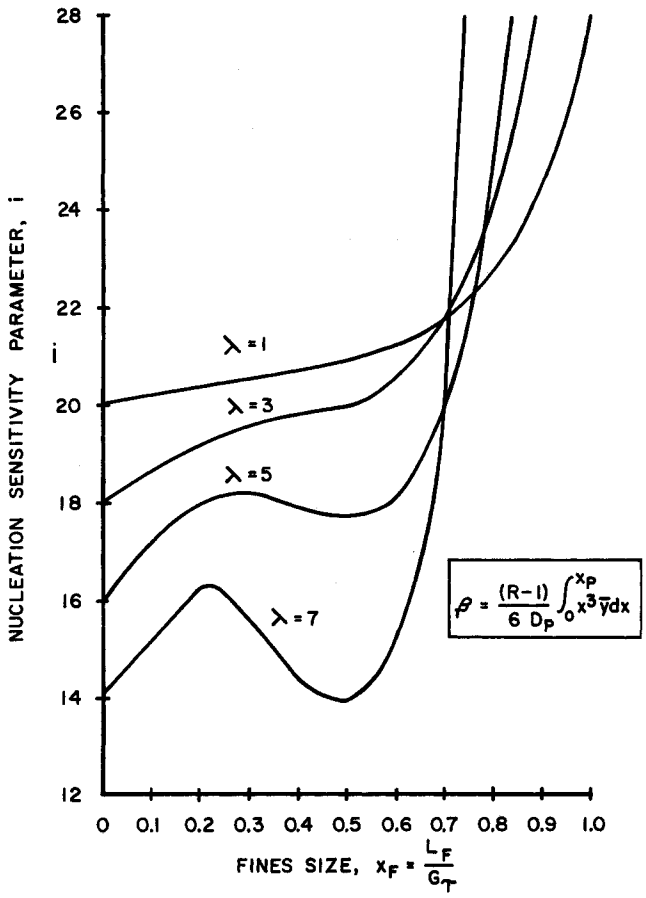

Fig. 5. Effect of fines size on CSD stability.

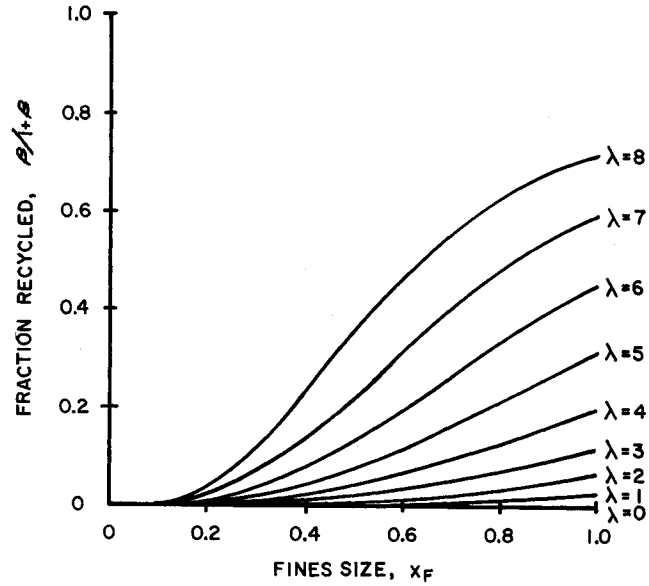

Fig. 6. Fraction of total internal make rate due to recycle of dissolved fines.

With any of these models, the weak destabilization of CSD caused by fines removal at small size does not explain low-order CSD cycling. Nucleation/growth rate sensitivity values measured over large ranges of driving forces in MSMPR crystallizers are typically in the range of 1 to 3. If fines removal indeed causes CSD cycling, the only reasonable explanation would seem to be that supersaturation was forced to a level where a discontinuous change in nucleation occurred, for example, by the sudden appearance of homogeneous nucleation.

Figure 6 shows the fraction of total internal make rate $\beta/1 + \beta$ due to recycle of dissolved fines as a function of fines size x_F and dissolving parameter λ. The fraction of solute recycled is only weakly dependent on the classification parameters x_p and z. The fraction of mass dissolved and recycled in a typical fines destruction system might range up to as high as 30 or 40% of the total rate of make. Such high mass recycle rates force the growth rate to higher levels unless compensating increases in crystallizer retention are made.

Effect of Product Classification

Figure 7 illustrates the dramatic effect of product classification in destabilizing CSD. These results are consistent with the extremely idealized classification model of Sherwin, Shinnar, and Katz. Two generalizations can be made from these stability calculations. First, the effect of accelerated product removal saturates at high z values (removal rate compared to MSMPR rate) above approximately 5 to 6. This observation supports the reasonableness of the infinite removal rate idealization used by Sherwin et al. Second, the destabilizing effects of classification are more pronounced at lower particle size x_p. Stability was scarcely effected when classification at $x_p = 10$ was assumed.

The mode and weight-averaged dimensionless sizes for the MSMPR distribution are 3.0 and 4.0, respectively. Classification narrows the product distribution and reduces average particle size. Thus, classification at dimensionless sizes such as illustrated in Figure 7 would still be at a size in excess of the average particle size. Figure 8 illustrates the lowering of average particle size (dimensionless) to be expected with product classification. Fines dissolving at

large x_F further lowers these dimensionless mean sizes. The effect of fines destruction is to raise the level of growth rate and hence increase the value of the dimensionalizing parameter G_T. Thus, a dimensionless product size of 2.5 to 3.0 could still represent a large absolute mean size. For example, assume a characteristic size parameter $G_T = 500\ \mu$ with classification due to nonisokinetic removal producing a mean suspension size of 1250μ ($\bar{x}_{susp} = 2.5$). From Figure 8 it is seen that only a small amount of classification (due to nonisokinetic removal) above 1500μ ($x_p = 3$) could easily produce such a narrowing of the distribution. Such amounts of classification at x_p values of about 3 would significantly destabilize the system as shown in Figure 7. Thus, it is conceivable that the amount of classification necessary to significantly lower the stability sensitivity limit would be achieved merely by nonisokinetic

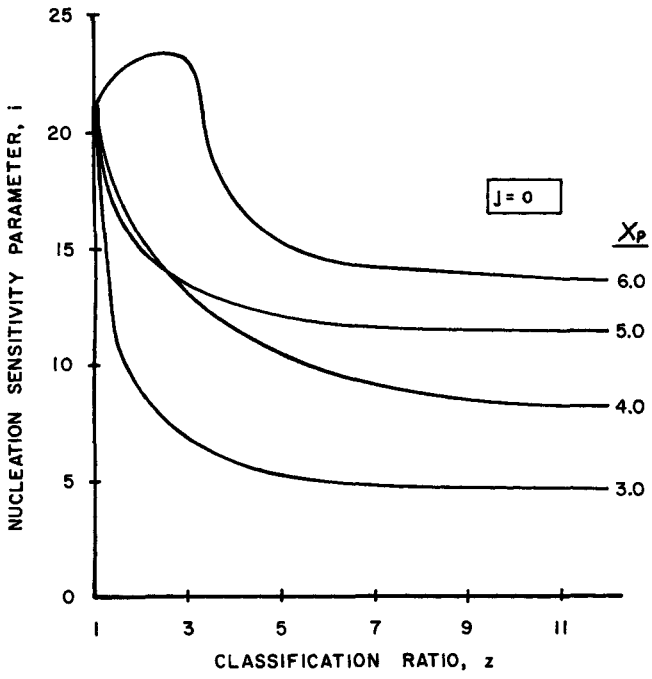

Fig. 7. Effect of product classification on CSD stability.

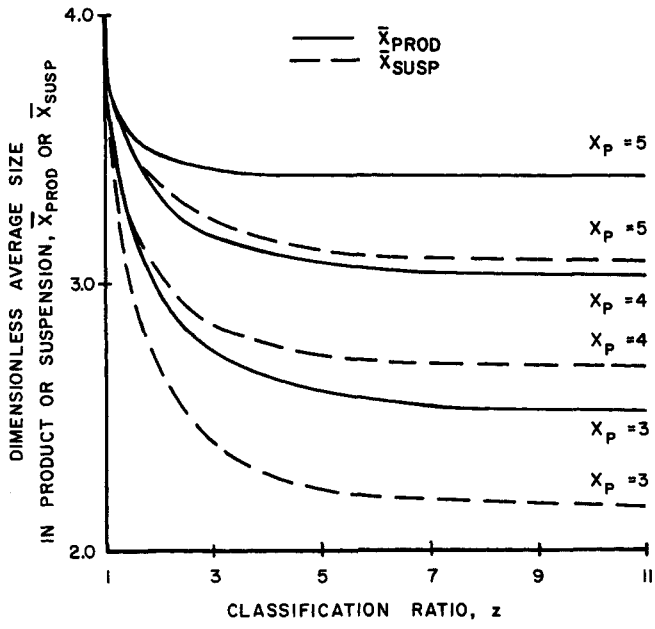

Fig. 8. Effect of product classification on mean particle size.

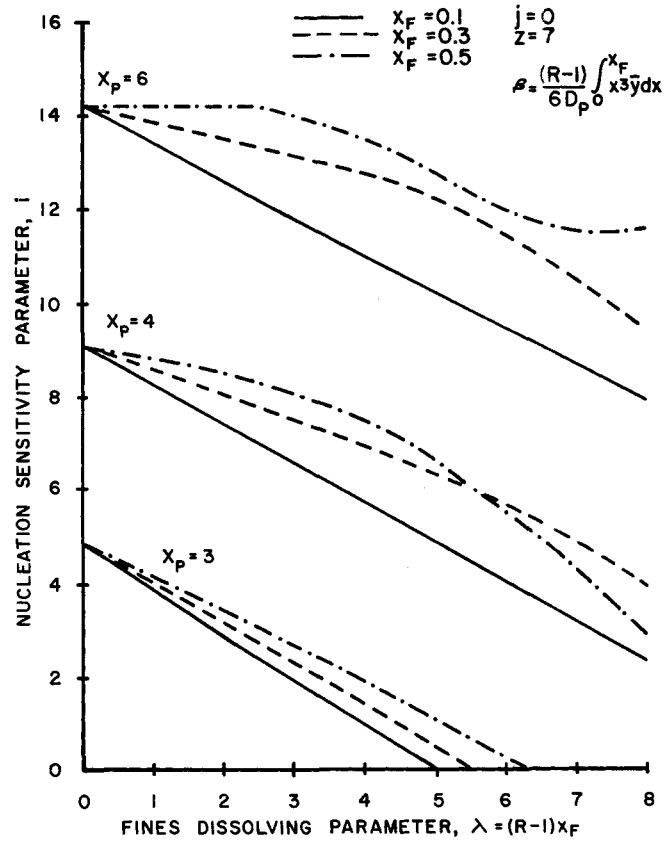

Fig. 9. Crystallizer stability for the R-z crystallizer with fines distribution and classified product removal (magma-independent nucleation).

product removal. Such amounts of classification could certainly be achieved with an external device, for example, wet screens.

Classification at low particle size and high rates (compared to mixed removal case) is thus seen as a possible source of low-order CSD cycling in mixed magma crystallizers.

Combination of Classification and Fines Removal

Figures 9 and 10 illustrate the combined effects of fines removal and product classification on CSD stability for various fines and classification sizes x_F and x_p as a function of the dissolving parameter λ and with recycle of fines. Figure 10 assumes magma-dependent kinetics given by $j = 1$. A high classification ratio of $z = 7$ was used in these calculations. This value is in the asymptotic region where further increases in z do not effect CSD. Dissolving fines at a larger size tends to stabilize the system, as indicated in Figures 9 and 10, but this effect is reduced with classification at low x_p values. Magma-dependent nucleation slightly stabilizes the system as seen by comparing Figure 10 with Figure 9. These figures indicate the low nucleation/growth rate sensitivity ratios that would result in CSD instability for the $R - z$ crystal distribution. Thus, a combination of classification and fines removal at small particle size could realistically explain the low-order cycling that has been observed in commercial crystallization machines.

The unfortunate interaction of fines dissolving and product classification to destabilize CSD goes deeper than the interaction shown in Figures 9 and 10. Excessive fines dissolving increases the absolute size of crystals produced and greatly increases the likelihood of classification due to nonisokinetic removal.

The modeling of process configuration and secondary

nucleation considered in this study is near the limit of our present understanding of crystallization processes. Still, severe product classification is necessary in every case to explain low-order CSD cycling. It is doubtful that this result, which is consistent with all previous work, would change with any further refinement in model description.

A final possibility for the explanation of low-order cycling might be due to severely size-dependent growth rates. Analysis of this situation would follow closely along the lines of present work. However, excluding the possibility of low growth rates for secondary nuclei (Randolph and Cise, 1972) there is no evidence for the grossly size-dependent crystal growth which might reasonably influence CSD stability.

Numerical Verification of CSD Stability

Nuttall (1971) presented results from a rigorous numerical computer program, the Mark III CSD simulator, in which he studied CSD transients after a step change in production for the Class II classified product crystallizer with fines destruction. Program Mark III solves the rigorous nonlinear CSD equations used as starting equations in this study. These numerical results can be used for direct comparison with the present linearized stability analysis. Nuttall made a case study of the classified fines removal crystallizer with and without recycle of dissolved fines mass. Table 2 summarizes the parameters used.

Figure 11 plots the response of CSD as the normalized third (mass) moment of the CSD after a step change in solute resources. The linearized stability study indicates that this crystallizer configuration, with the given parameters, should be unstable (fines mass recycled) with a nucleation/growth rate sensitivity of $i = 5.9$. The direct numerical computations of Nuttall indicated that cycling began with a nucleation/growth rate sensitivity approximately $i = 6$. Both the direct numerical simulation and the linearized stability analysis predict a stable CSD when fines mass from the dissolver was not recycled, as shown in Figure 11.

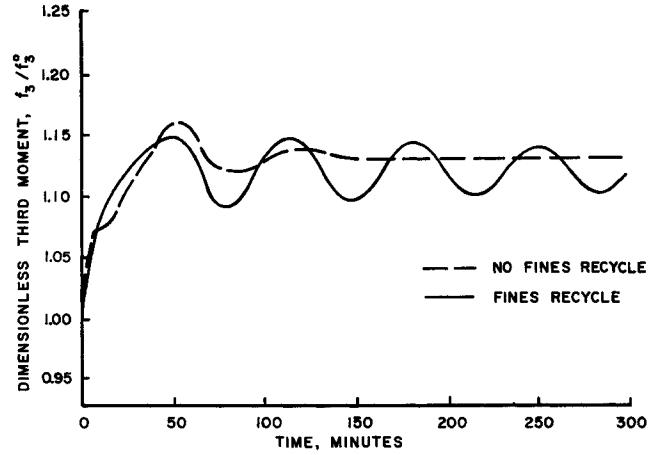

Fig. 11. Response of third moment of CSD to step change in solute resources for the classified crystallizer with fines destruction.

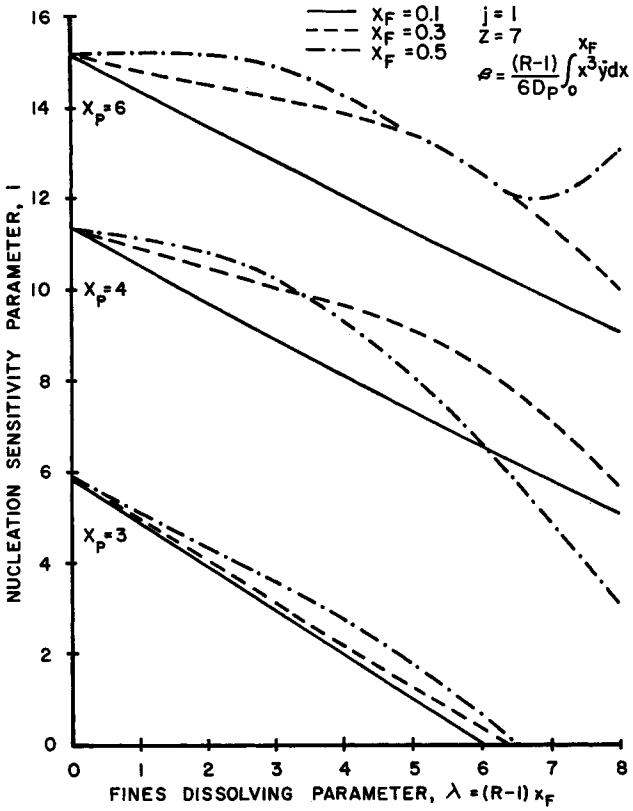

Fig. 10. Crystallizer stability for the R-z crystallizer with fines destruction and classified product removal (magma-dependent nucleation).

Table 2. Parameters and Results of Mark III CSD Simulation

Parameter	Fines recycle	No fines recycle
x_F	1.0	1.0
x_p	3.0	3.0
R	5	5
z	5	5
i, Mark III	6.0	6.0
i, Stability limit	5.9	∞
Computed CSD stability	Marginally unstable	Completely stable
Stability prediction	Marginally unstable	Completely stable

ACKNOWLEDGMENT

The authors gratefully acknowledge the financial assistance provided by the National Science Foundation through Grants GK-10551 and 36517X.

NOTATION

$A(t)$ = crystal area in suspension
b = search variable $Im(s) = b$
B^0 = nucleation rate
C = concentration in crystallizer
C_i = concentration in feed
C_s = saturation concentration
D, D_p = dimensionless functions in steady state growth rate equation
$f_{j,K}$ = dimensionless normalized moments of distribution growth rate equation
G, G_0 = dynamic and steady state growth rates
$G(x)$, G_α^n = integral functions used in spectral analysis
$h(L)$ = removal function
$H(x)$, H_α^n = integral functions used in spectral analysis
i = nucleation growth rate kinetic sensitivity parameter
j = magma-dependent nucleation kinetics exponent
K_N = nucleation constant

K_v = shape factor for volume
L = characteristic particle size
L_F = particle size at upper limit of fines destruction
L_p = particle size at lower limit of classification
MSMPR = mixed suspension mixed product removal
M_T = solids concentration
$n(L,t)$, $n_0(L)$ = dynamic and steady state number density function
n^0, n_0^0 = dynamic and steady state nuclei density
P_I = internal production rate
P_E = external production rate
Q = flow rate through crystallizer
R = ratio of total fines removal rate (product plus fines trap) to flow through crystallizer
s = spectral variable
t = time
V = crystallizer volume
x = dimensionless particle size
x_F, x_p = dimensionless size limits for fines removal or classification
y = dimensionless number density
$\bar{y}$ = steady state dimensionless number density
y^0 = dimensionless nuclei density
Y_α^n = integral over y used in spectral analysis
z = ratio of classified product removal to flow through crystallizer

Greek Letters

β = ratio of fines destruction to external production
ϕ = dimensionless growth rate
λ = dissolving parameter, $(R-1)x_F$
ρ = crystal density
θ = dimensionless time
τ = residence time based on mixed removal rate

LITERATURE CITED

Hulburt, H. M., and D. G. Stefango, "Design Models for Continuous Crystallizers with Double Draw-Off," *Chem. Eng. Prog. Symp. Ser. No. 95*, **65**, 50 (1969).

Lie, S. J., R. Shinnar, and S. Katz, "The Stability and Dynamic Behavior of a Continuous Crystallizer with Fines Trap," *AIChE J.*, **17**, 1459 (1971).

———., "Feedback Control of a Continuous Crystallizer With and Without Fines Trap," *Chem. Eng. Prog. Symp. Ser. No. 110*, **67**, 129 (1971).

Randolph, A. D., "Size Distribution Dynamics in a Mixed Suspension," Ph.D. thesis, Iowa State Univ. of Science Tech., Ames, Iowa (1962).

———., and M. D. Cise, "Nucleation Kinetics of the Potassium Sulfate-Water System," *AIChE J.*, **18**, 798 (1972).

Randolph, A. D. and M. A. Larson, "Theory of Particulate Processes," pp. 83, 97, 142, 231, Ch. 5, Academic Press, New York (1971).

Sherwin, M., R. Shinnar, and S. Katz, "Dynamic Behavior of the Isothermal Well-Stirred Crystallizer with Classified Outlet," *Chem. Eng. Symp. Ser. No. 95*, **65**, 75 (1969).

APPENDIX

We outline here the derivation of the characteristic Equation (15) for the linearized Equation (14), which we write as

$$\left.\begin{aligned} \frac{\partial y}{\partial \theta} &= \frac{\beta}{1+\beta} h\,\bar{y}\,f_{3,1} - h\,\bar{y}\,f_2 - \frac{\partial y}{\partial x} - hy, \\ \text{with boundary condition} \quad & \\ y^0 &= jf_3 + \left(\frac{i-1}{1+\beta}\right)\beta f_{3,1} - (i-1)f_2. \end{aligned}\right\} \quad \text{(A1)}$$

We seek solutions of this equation in the form $y(\theta,x) = e^{-s\theta}u(x)$. These solutions, when they exist, will be stable if $Re(s) > 0$, unstable if $Re(s) < 0$, with the transition obviously occurring when $Re(s) = 0$. Furthermore, all solutions of (A1) can be represented as an appropriate linear combination of the spectral solutions $e^{-s\theta}u_s(x)$.

Using this special representation for $y(\theta,x)$, Equation (A1) becomes

$$\left.\begin{aligned} &\frac{du}{dx} + (h(x)-s)u = \left(\frac{\beta}{1+\beta}F_{3,1} - F_2\right) h(x)\,\bar{y}\,(x) \\ &u(0) = jF_3 + \left(\frac{i-1}{\beta+1}\right)\beta F_{3,1} - (i-1)F_2 \\ &\text{where} \\ &F_{3,1} = \frac{\int_0^{x_F} x^3 u(x)dx}{\int_0^{x_F} x^3\,\bar{y}\,(x)dx}; \quad F_k = \frac{\int_0^{\infty} x^k u(x)dx}{\int_0^{\infty} x^k\,\bar{y}\,(x)dx}, \quad k = 2, 3, \end{aligned}\right\} \quad \text{(A2)}$$

Since (A2) is a first-order ordinary differential equation, it can be solved explicitly to get

$$\left.\begin{aligned} u(x) = &\left(jF_3 + (i-1)\frac{\beta}{\beta+1}F_{3,1} - (i-1)F_2\right)H(x) + \left(\frac{\beta}{\beta+1}F_{3,1} - F_2\right) H(x)G(x) \\ &\text{where} \\ H(x) &= \exp\left(sx - \int_0^x h(\tau)d\tau\right); \\ G(x) &= \int_0^x h(\tau)e^{-s\tau}\,d\tau \end{aligned}\right\} \quad \text{(A3)}$$

The expression for $G(x)$ takes into account that

$$\bar{y}\,(x) = \exp\left(-\int_0^x h(\tau)d\tau\right) \quad \text{(A4)}$$

Computing $F_{3,1}$, F_2, and F_3 in (A2) by means of (A3) gives the set of three equations

$$\left.\begin{aligned} Y_\infty^k F_k = &\left(jF_3 + (i-1)\frac{\beta}{\beta+1}F_{3,1} - (i-1)F_2\right)\mathcal{H}_\infty^k + \left(\frac{\beta}{\beta+1}F_{3,1} - F_2\right)\mathcal{G}_\infty^k, \quad k = 2, 3 \\ Y_{x_F}{}^3 F_{3,1} = &\left(jF_3 + (i-1)\frac{\beta}{\beta+1}F_{3,1} - (i-1)F_2\right)\mathcal{H}_{x_F}{}^3 + \left(\frac{\beta}{\beta+1}F_{3,1} - F_2\right)\mathcal{G}_{x_F}{}^3 \\ &\text{where} \\ \mathcal{H}_\alpha^k &= \int_0^\alpha x^k H(x)dx; \quad \mathcal{G}_\alpha^k = \int_0^\alpha x^k H(x)G(x)dx; \\ Y_\alpha^k &= \int_0^\alpha x^k\,\bar{y}\,(x)dx \end{aligned}\right\} \quad \text{(A5)}$$

The Equations (A5) comprise a set of three homogeneous linear equations in the three unknowns $F_{3,1}$, F_2, and F_3, which can be written as

$$(A - Y)\begin{bmatrix} F_1 \\ F_2 \\ F_3 \end{bmatrix} = 0 \quad \text{(A6)}$$

with $A = (a_{kl})$ given by

$$\left.\begin{aligned} a_{k1} &= (i-1)\frac{\beta}{\beta+1}\eta_k + \frac{\beta}{\beta+1}\gamma_k \\ a_{k2} &= -(i-1)\eta_k - \gamma_k \\ a_{k3} &= \eta_k \end{aligned}\right\} \quad k = 1, 2, 3 \qquad \text{(A7)}$$

$$Y = \begin{bmatrix} Y_{xF}{}^3 & 0 & 0 \\ 0 & Y_x{}^2 & 0 \\ 0 & 0 & Y_x{}^3 \end{bmatrix} \qquad \text{(A8)}$$

where for notational convenience we have used

$$\left.\begin{aligned} \eta_1 &\equiv \mathcal{H}_{xF}{}^3, \quad \gamma_1 \equiv \mathcal{G}_{xF}{}^3, \quad F_1 \equiv F_{3,1} \\ \eta_k &\equiv \mathcal{H}_x{}^k, \quad \gamma_k \equiv \mathcal{G}_x{}^k, \quad k = 2, 3 \end{aligned}\right\} \qquad \text{(A9)}$$

In order to find a nontrivial solution of (A6), we require

$$\det(A - Y) = 0 \qquad \text{(A10)}$$

which is the characteristic equation for s. Equation (15) follows from (A7) to (A10) by standard manipulation.

Manuscript received April 10, 1973; revision received and accepted May 17, 1973.

Water Jet Atomization of Molten Steel

Data are obtained and a model derived for describing particle size distribution for molten metals atomized by two water jets. The influences of water jet parameters on size distribution and median size are reported and discussed in terms of fundamental quantities and model predictions. The data, which were obtained using fan-spray jets impinging at an apex angle of 60° to atomize Type 4620 steel, indicated that median size was primarily a function of water jet velocity.

RICHARD J. GRANDZOL and JOHN A. TALLMADGE

Department of Chemical Engineering
Drexel University
Philadelphia, Pennsylvania 19104

SCOPE

This paper is concerned with the description of the atomization of molten metals by impinging water jets. This process is a major method for production of metal powders which are used increasingly in manufacture of precision parts by powder metallurgy. The geometry of concern involves a two-liquid system which is more flexible and more suitable for molten metals than the usual one-liquid atomization methods, two of which are use of rotating disk or a pressured nozzle. As compared with isothermal atomization of organic and aqueous liquids, the quench aspect of cooling the molten metal is desirable from an experimental standpoint because the resultant particles are obtained in solid form; this permits simple determination of the size distributions instead of the complex methods needed for fluid droplets.

There is considerable empirical work on the atomization of aqueous and organic liquids by a gas stream, as noted in the summary by Lapple et al. (1967). However, little work on water jet atomization of liquids has been published. Studies by Small and Bruce (1968), Gummeson (1972), and others indicate that the median size and other properties of powders formed by water and gas atomization differ to a large degree; thus it is apparent that the work for gas atomization is not suitable for description of water atomization. Hence an analysis of water atomization of liquid metals would be useful, especially if prediction models are developed and compared with precise data.

The two main objectives of this paper are to describe the median size of metal powders in two ways, experimentally and with a model, using two-jet atomization of molten 4620 steel. As part of this, the influence of several jet parameters was studied in order to determine which ones were primary, secondary, or negligible in their effect on median size and size distribution. The water jet parameters studied included pressure, momentum, energy, velocity, flow rate, and jet length. The influence of metal flow rate was studied by varying the diameter of the molten metal stream. The model approach is based on conservation of momentum and energy balances for the dispersed water droplets, supplemented with data from other measurements.

CONCLUSIONS AND SIGNIFICANCE

Atomization data show that water droplet velocity (V_w) is the fundamental variable influencing median size of the metal particle (d_m). The following functional form was observed (Figure 7), where A is a constant:

$$d_m = A/V_w \qquad (1)$$

Throughout this work, median size refers to the mass median particle diameter (or volume median since density was considered to be constant). Over the ranges studied, it was also found that water pressure, momentum, and energy were not primary parameters influencing median size but did affect size by influencing water jet velocities.

Correspondence concerning this paper should be addressed to J. A. Tallmadge.